


A Comparison of Iron Oxide Particles and Silica Particles for Tracking Organ Recellularization

Joseph E. Kobes, MS^{1,2}, George I. Georgiev, MS¹, Anthony V. Louis, MD³, Isen A. Calderon, PhD⁴, Eriko S. Yoshimaru, PhD¹, Louie M. Klemm, MS³, Douglas W. Cromey, MS⁵ , Zain Khalpey, MD, PhD³, and Mark D. Pagel, PhD^{1,4,5}

Abstract

Reseeding of decellularized organ scaffolds with a patient's own cells has promise for eliminating graft versus host disease. This study investigated whether ultrasound imaging or magnetic resonance imaging (MRI) can track the reseeded of murine liver scaffolds with silica-labeled or iron-labeled liver hepatocytes. Mesoporous silica particles were created using the Stöber method, loaded with Alexa Fluor 647 fluorophore, and conjugated with protamine sulfate, glutamine, and glycine. Fluorescent iron oxide particles were obtained from a commercial source. Liver cells from donor mice were loaded with the silica particles or iron oxide particles. Donor livers were decellularized and reperfused with silica-labeled or iron-labeled cells. The reseeded livers were longitudinally analyzed with ultrasound imaging and MRI. Liver biopsies were imaged with confocal microscopy and scanning electron microscopy. Ultrasound imaging had a detection limit of 0.28 mg/mL, while MRI had a lower detection limit of 0.08 mg/mL based on particle weight. The silica-loaded cells proliferated at a slower rate compared to iron-loaded cells. Ultrasound imaging, MRI, and confocal microscopy underestimated cell numbers relative to scanning electron microscopy. Ultrasound imaging had the greatest underestimation due to coarse resolution compared to the other imaging modalities. Despite this underestimation, both ultrasound imaging and MRI successfully tracked the longitudinal recellularization of liver scaffolds.

Keywords

iron oxide particles, silica particles, magnetic resonance imaging, ultrasound imaging, organ recellularization

Introduction

Allograft organ transplantation from a donor to a recipient is one of the most challenging and complex medical procedures employed to address many common medical problems when other treatment options have failed. Although great progress has been made to improve donor organ engraftment, immunogenic rejection of an organ from an unrelated donor remains problematic.¹ To address this problem, substantial progress has been made in tissue engineering research involving the decellularization of donor organs, which can subsequently be repopulated with a recipient's cells from the same organ.² This approach has great potential to revolutionize autologous organ transplantation, where cells or tissue from a patient are transplanted to a new location in the same patient.

The liver is the second most common organ used in allograft transplantations.³ Due to the increase in liver pathologies such as nonalcoholic fatty liver disease, nonalcoholic

steatohepatitis, and hepatocellular carcinoma, liver transplantations have potential to become more common than kidney transplants.^{4,5} Thus, substantial tissue engineering efforts have

¹ Department of Biomedical Engineering, University of Arizona, Tucson, AZ, USA

² Department of Chemistry and Life Science, United States Military Academy, West Point, NY, USA

³ Department of Surgery, University of Arizona, Tucson, AZ, USA

⁴ Department of Chemistry and Biochemistry, University of Arizona, Tucson, AZ, USA

⁵ University of Arizona Cancer Center, University of Arizona, Tucson, AZ, USA

Submitted: 22/08/2017. Revised: 31/10/2017. Accepted: 07/03/2018.

Corresponding Author:

Mark D. Pagel, University of Texas MD Anderson Cancer Center, 35CR4.3642, 1881 East Road, Houston, TX 77054, USA.

Email: mdpagel@mdanderson.org



particularly focused on the de/recolonization of liver tissues from a range of animal models. However, improvements are needed to reseed and proliferate recipient liver cells throughout the decellularized liver scaffold from a donor. This process of cell reseeding and proliferation would benefit from noninvasive methods that can track this process.

Noninvasive imaging provides strong advantages for evaluating the longitudinal progression of organ recolonization. Ultrasound imaging with a high frequency transducer can produce images with $\sim 125 \mu\text{m}$ spatial resolution in 3 dimensions and can be rapidly performed within seconds after a few minutes of preparation time.⁶ Mesoporous silica particles are echogenic materials that produce strong ultrasound imaging signals relative to background, which have been used for a variety of molecular imaging applications including cell labeling due to the long-term stability of these particles in cells.^{7,8} For comparison, magnetic resonance imaging (MRI) at a high magnetic field strength and a small-diameter transceiver coil can generate $50 \mu\text{m}$ spatial resolution in 3 dimensions.⁹ With proper expertise, MR imaging of tissue samples can be performed within 10 minutes. Iron oxide particles generate darker image contrast via T_2^* relaxation and have been employed for many molecular imaging studies.^{10,11} In particular, iron-labeled cells have been tracked in vivo for many biomedical studies.¹²

We investigated the use of ultrasound imaging and MRI to detect and monitor the recolonization of liver scaffolds. We characterized mesoporous silica particles and iron oxide particles, especially to determine their detection sensitivity with their respective imaging modality. We then labeled liver cells with each type of particle, decellularized and reseeded liver scaffolds with the labeled cells, and monitored longitudinal cell proliferation. We included fluorophores in each particle so that we could employ confocal microscopy of biopsied liver samples. We also used scanning electron microscopy (SEM) of biopsied samples to evaluate the progression and quantity of recolonizations.

Materials and Methods

Reagents

All reagents were obtained from Sigma-Aldrich (St. Louis, Missouri) unless otherwise specified. The synthesis of silica particles used tetraethyl orthosilicate, ammonium hydroxide (EMD Millipore Corp, Billerica, Massachusetts), 200 proof ethanol (Decon Labs, Inc, King of Prussia, Pennsylvania), and Alexa Fluor 647 (Invitrogen, Thermo Fisher Scientific, Inc, Grand Island, New York). The silica particles were modified using 90% nitric acid, 99.9% anhydrous acetonitrile (Acros Organics, Geel, Belgium), 99% (3-aminopropyl)triethoxysilane (APTES), 200 proof ethanol (Decon Labs, Inc), phosphate-buffered saline (PBS; G-Biosciences, Inc, St. Louis, Missouri), protamine sulfate, acetone (Fisher Scientific, Pittsburgh, Pennsylvania), L-glutamine, agar (Difco, Becton Dickson Co, Franklin Lakes, New Jersey), 2-(N-morpholino)ethanesulfonic acid buffer (MES), water soluble carbodiimide (Acros Organics), 99% N, N'-dicyclohexyl-carbodiimide

(G-Biosciences, Inc), and Tween 20 (EMD Millipore Corp). Polystyrene particles with an average diameter of $1.63 \mu\text{m}$ contained iron oxide particles and Dragon Green fluorophore (Bangs Laboratories, Inc, Fishers, Indiana).

Cell culture supplies included MEM Alpha with GlutaMAX (Gibco, Thermo Fisher Scientific, Inc), a solution of 10 000 units/mL penicillin and 10 000 $\mu\text{g}/\text{mL}$ streptomycin (HyClone, GE Healthcare Life Sciences, Inc, Logan, Utah), fetal bovine serum (FBS), and trypsin with $1 \times$ EDTA in 0.25% Hank's Balanced Salt Solution (HBSS) (Corning, Inc, Pittsburgh, Pennsylvania). Tissue processing was accomplished with 4% (wt/vol) paraformaldehyde (EMD Millipore Corp), University of Wisconsin (UW) organ preservation solution (Preservation Solutions, Inc., Elkhorn, Wisconsin), 70- μm Falcon nylon filters (Becton Dickson Co), collagenase, collagen I bovine protein (Gibco, Thermo Fisher Scientific, Inc), and percoll density centrifuge gradient media.

Particle Synthesis

Silica mesoporous particles were synthesized using the Stöber method with minor changes.¹³ Particles were synthesized by quickly adding a solution of 50 μg of Alexa Fluor 647 in 2 mL of tetraethoxysilane (TEOS) and 3 mL of ethanol to a stirred solution of 2.5 mL ammonia in 23.5 mL ethanol under argon gas at room temperature. The solution was stirred for 1 hour and sonicated for 10 minutes. The particles were then centrifuged at 8000 rpm (2135g) for 30 minutes, washed with water, vortexed, sonicated, and resuspended in water, for a total of 3 times. To quantify particles produced during synthesis, 20% of the final suspension dissolved in deionized water was added to an Eppendorf tube of known weight, lyophilized, and reweighed.

Particle Modification

The surfaces of the silica mesoporous particles were modified to improve cellular uptake.¹⁴ More specifically, the unmodified silica nanoparticles had a surface with a high negative charge. Modification of the surface with protamine sulfate, glutamine, and glycine reduced this negative charge, which improves cellular uptake. One milliliter of silica mesoporous particles at 12.68 mg/mL concentration was centrifuged at 10 000 rpm (3335g) for 10 minutes. The pellet was resuspended in 10 mL of 1 mol/L nitric acid, sonicated for 10 minutes, and heated to 70°C to 80°C for 30 minutes. To remove the nitric acid, the solution was centrifuged, resuspended in water, and sonicated for 10 minutes 3 times. To remove the water, the particles were centrifuged, washed in acetone, and sonicated for 10 minutes 3 times. To remove the acetone, the particles were dried under argon gas and kept in an oven at 70°C for 30 minutes.

To conjugate APTES to the surface, the particles were resuspended in 2 mL of APTES and shaken for 12 hours. The silica particles were centrifuged at 10 000 rpm for 10 minutes and resuspended in acetonitrile 3 times, then centrifuged and resuspended in ethanol 3 times, and finally centrifuged and resuspended in deionized water 3 times.

To further derivatize the surface of the particles, the silica particles were centrifuged at 10 000 rpm for 10 minutes and resuspended in 5 mL deionized water with a 10% solution of N-hydroxysuccinimide ester crosslinker for 2 hours at room temperature. After the crosslinker was conjugated to the surface, the silica particles were centrifuged at 10 000 rpm for 10 minutes, resuspended in 0.112% (wt/vol) protamine sulfate with 10 mL PBS 1× buffer, and reacted for 4 hours at room temperature. The silica particles were centrifuged at 10 000 rpm for 10 minutes and resuspended in 40 mmol/L solution of glutamine and 13.32 mmol/L glycine blocking solution with 10 mL PBS 1× buffer to quench the reaction. The silica particles were centrifuged at 10 000 rpm for 10 minutes and resuspended 3 times in deionized water with a final volume of 10 mL. From the final volume, 2 mL of the suspension were placed in an Eppendorf tube of known weight, lyophilized, and reweighed to determine the final yield.

The iron oxide particles had a polystyrene coating that included Dragon Green fluorophore and were found to have an average diameter of 1.63 μm . These iron oxide particles were modified with protamine sulfate to improve cell uptake.¹⁵ One milliliter of 100 mg/mL iron oxide particles was centrifuged at 5500 rpm (1008g) for 10 minutes. To sterilize the material, the particles were resuspended in 1 mL of ethanol, vortexed, and centrifuged at 5500 rpm for 10 minutes for a total of 3 times. The particles were resuspended in 1 mL of distilled water, vortexed, sonicated for 5 minutes, and centrifuged at 10 000 rpm for 10 minutes for a total of 3 times. The particle solution was centrifuged at 10 000 rpm for 10 minutes and resuspended in 10 mL of the MES activation buffer at pH 6.22 for a total of 2 times using vortexing, water bath sonication, and centrifugation, followed by incubation for 24 hours at 4°C. The particles were centrifuged at 10 000 rpm for 10 minutes, and the pelleted particles were resuspended in 10 mL of the activation buffer with 64.8 mmol/L of water soluble carbodiimide at room temperature for 15 minutes. The particles were then washed in the PBS coupling buffer 2 times following the same vortex, centrifuge, and sonication techniques, then incubated in 5 mL of the coupling buffer with a 2.55 mmol/L protamine sulfate, and allowed to react at room temperature for 4 hours. The particles were centrifuged, and the pellet was resuspended in a solution of 14.6 mmol/L glutamine in 10 mL PBS quenching solution and mixed for 30 minutes. The particles were centrifuged, supernatant was removed, and the particles were resuspended in PBS storage buffer at 4°C.

Particle Characterization

The dynamic light scattering (DLS) of the particles was measured in triplicate using a Zetasizer Nano Series system (Malvern Instruments, Ltd, Malvern, United Kingdom). Samples of 200 $\mu\text{g}/\text{mL}$ of silica particles or iron oxide particles were analyzed in triplicate. The refraction index was set to 1.45 for silica particles, 2.42 for iron oxide particles, and 1.332 for PBS. These refractive indices were preset by Malvern and selected for their similarity to our materials.

Cell Isolation and Labeling

Murine liver hepatocytes were isolated from C.B-17/Icr ACC SCID mice using a combination of previously reported methods.¹⁶⁻²¹ Upon mouse killing and liver extraction, the liver was placed in UW organ preservation solution at 37°C. The tissue was minced with a razor and treated with 6 mL of 1.1 mg/mL collagenase at 37°C for 6 to 10 minutes with periodic shaking. After digestion was complete, the contents were filtered through a 70- μm nylon filter into 15 mL of cold Alpha MEM media, which was centrifuged at 1100 rpm (40g) for 5 minutes at room temperature. The supernatant was recentrifuged, and the 2 pellets were combined and resuspended in complete Alpha MEM media, 10% FBS, and 1% PenStrep (100 U/mL penicillin and 100 $\mu\text{g}/\text{mL}$ streptomycin). The cells were then incubated at 37°C and 5% CO_2 .

To label cells with particles, liver cells were grown to 80% confluency, trypsinized for 6 to 8 minutes at 37°C, and regrown to 75% confluency.²² Cells were washed once with $\text{Mg}^+/\text{Ca}^{2+}$ -free 1× PBS and treated with 650 μL of a 4.3 mg/mL solution of silica- or iron-based particles in Alpha MEM media and 2× P/S with no serum. The particles were incubated with the cells for 3 hours, then 700 μL of FBS was added to the cells. After incubation for an additional 17 hours, the particle solution was aspirated, the cells were washed with prewarmed $\text{Mg}^+/\text{Ca}^{2+}$ -free 1× PBS, and 7 mL of complete media were added to the cells.

Liver Decellularization, Recellularization, and Analyses

All animal procedures were conducted with approval from the Institutional Animal Care and Use Committee of the University of Arizona. Three livers were tested with ultrasound imaging, and 3 other livers were tested with MRI. To decellularize the liver, a mouse was killed, the liver was extracted, and the liver was placed in UW solution at 37°C (Figure 1).²³ The liver was agitated via vortex in 15 mL of hypotonic solution for 15 minutes. Then, the liver was removed from the deionized water, agitated in 15 mL of 1× PBS for 30 minutes, and immersed in a 10% (vol/vol) solution of Triton X-100 in deionized water for several hours to decellularize the tissue. The decellularized liver was removed from the Triton X-100 solution and agitated in 1× PBS for 15 minutes for 3 times to complete the decellularization process.

To recellularize the liver scaffold, approximately 1 million particle-loaded liver cells were gently aspirated and washed with $\text{Mg}^+/\text{Ca}^{2+}$ -free 1× PBS. The cells were then quickly washed with 3 mL of 0.25% trypsin, and then treated with 7 mL of 0.25% trypsin for 6 to 10 minutes to remove the cells from the surface of the container. Cold media was added to the cells to bring the total volume to 14 mL. The conical tube was centrifuged at 1100 rpm for 5 minutes, and the cell pellet was reconstituted in 5 mL complete media and injected into the portal vein of a decellularized liver with a 27 g needle. The cell solution that was reperfused through the liver was collected and reinjected for a total of 6 to 10 times.

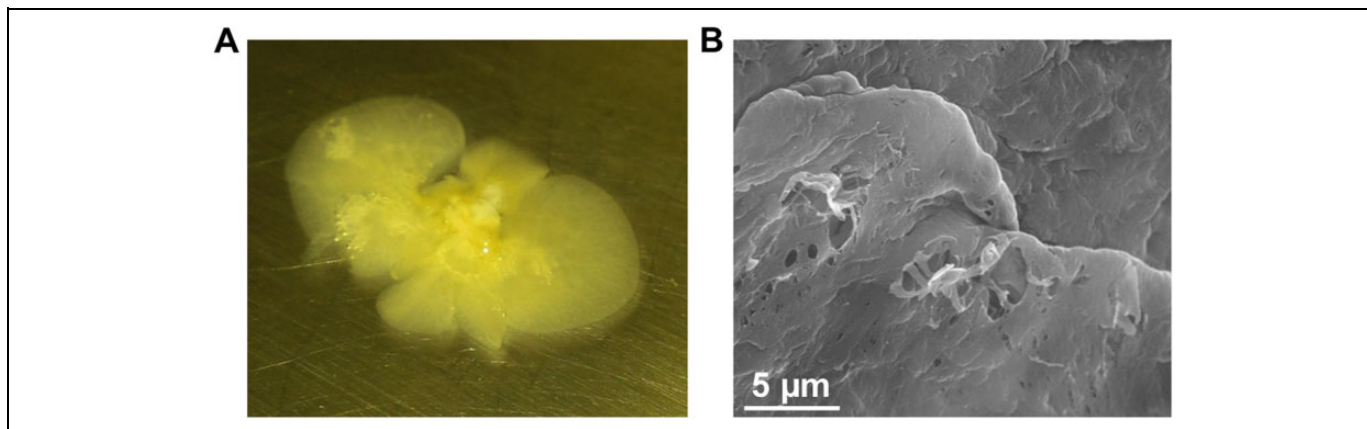


Figure 1. Decellularization of mouse liver. A, A photograph of an excised mouse liver before decellularization showed an abundance of cells. B, An SEM image of the decellularized tissue verified that cells were absent and the scaffold retained structural integrity.

Reseeded livers were placed in 50-mL conical tubes incubated at 37°C in a ThermoForma Series II CO incubator that included a water jacket and high-efficiency particulate air (HEPA) filter (Thermo Scientific, Inc, Waltham, Massachusetts). The enclosed incubator had an atmosphere of 5% CO₂, and the conical tubes tops were loosened to ensure air exchange. The livers were maintained in Alpha MEM media with 10% FBS and 1% PenStrep, and this media was changed every 2 days. Conical tubes were removed from the incubators for 5 to 10 minutes to remove a biopsy slice in a sterile environment and then the livers were returned to the incubator. Biopsied tissues were fixed in paraformaldehyde prior to further analysis.

Ultrasound images of the intact liver were obtained at 0, 1, 7, 11, 14, 21, and 27 days postseeding. Magnetic resonance imaging scans were performed with the liver scaffold on day 1 before cell reperfusion and on days 4, 10, 17, and 31 after cell reperfusion. Liver biopsies were imaged by confocal microscopy on days 1, 9, 13, and 29 for silica-labeled livers and on days 1, 9, 11, 13, 20, and 31 for iron-labeled livers. Biopsy samples of the silica-labeled cells were imaged with SEM on days 0, 7, 9, 13, 19, and 29. Biopsies of the iron-labeled cells were imaged with SEM on days 0, 7, 9, 13, 19, and 29. These measurements were volumetrically normalized.

Imaging Studies

Ultrasound images were acquired using a Vevo 2100 scanner with a linear transceiver array operating at 50 MHz (Visualsonics, Inc, Toronto, ON, Canada). To determine the theoretical lower limit of detecting silica particles with ultrasound imaging, we mixed 0.2, 0.4, 1.32, and 1.56 mg/mL concentrations of silica particles in 10% (wt/vol) agar. The average ultrasound intensity was measured 7 mm deep into each sample, then each sample was sliced every 2 mm and imaged in the confocal microscope to verify particle location and differentiation from any remaining bubbles in the solidified sample. To determine the number of particles, the grayscale of the ultrasound images were inverted so the brighter spots became dark. The Image-based Tool for Counting Nuclei plugin within ImageJ (ImageJ

version 1.49) was used with an empirically determined minimum threshold and the average particle diameter to automatically calculate the number of silica-labeled cells.²⁴

To analyze tissues with ultrasound imaging, the liver was placed in a customized nylon container with a 10% agar bottom so that the liver could be imaged from the bottom of the container while the liver was in cell media. The same analysis protocol with ImageJ described above was used to estimate the number of cells or cell groups in the liver. The area of the liver in each 2D image slice was used to estimate 3D liver volume to provide a volumetric count of cells labeled with silica particles.

Magnetic resonance imaging was used to analyze iron oxide particles in agar. Magnetic resonance imaging was also used to image the same liver samples that were evaluated with ultrasound imaging. T₂-weighted MR images were acquired using a Biospec MRI scanner with a 4-channel array coil in a 7T magnet with a 20-cm bore (Bruker Biospin, Inc, Billerica, Massachusetts).²⁵ A spin-echo acquisition protocol was performed with 6000 ms TR, 40 to 480 ms TE, 12 echoes, 2.77 × 2.77 cm field of view, 54 × 54 μm in-plane resolution, 0.5-mm slice thickness, 4 slices, and 2 averages at 37°C. Data from samples that ranged between 0.14 and 10.7 mg/mL were analyzed to determine the T₂ relaxivity of the iron oxide particles. T₂ parametric maps were calculated using Paravision v. 5.1 (Bruker Biospin, Inc). The same analysis protocol with ImageJ described above was used to estimate the number of cells or cell groups in the liver.

A SP5-II spectral confocal microscope (Leica Microsystems, Buffalo Grove, Illinois) used a 633-nm Helium Neon laser to image silica particles labeled with Dragon Green fluorophore, and used a 488-nm argon laser to image iron oxide particles labeled with the same fluorophore. The objective lenses used for imaging were the 10×/0.4 PL Apo, 20×/0.7NA Plan Apo, 20×/0.7NA Plan Apo multi-IMM (oil), 40×/1.25NA PL Apo (oil), and 63×/1.4 NA PL Apo (oil). The microscope had an inverted stand with an environmental control chamber for live cell imaging. The images were processed using Leica's LAS-AF software version 2.7.

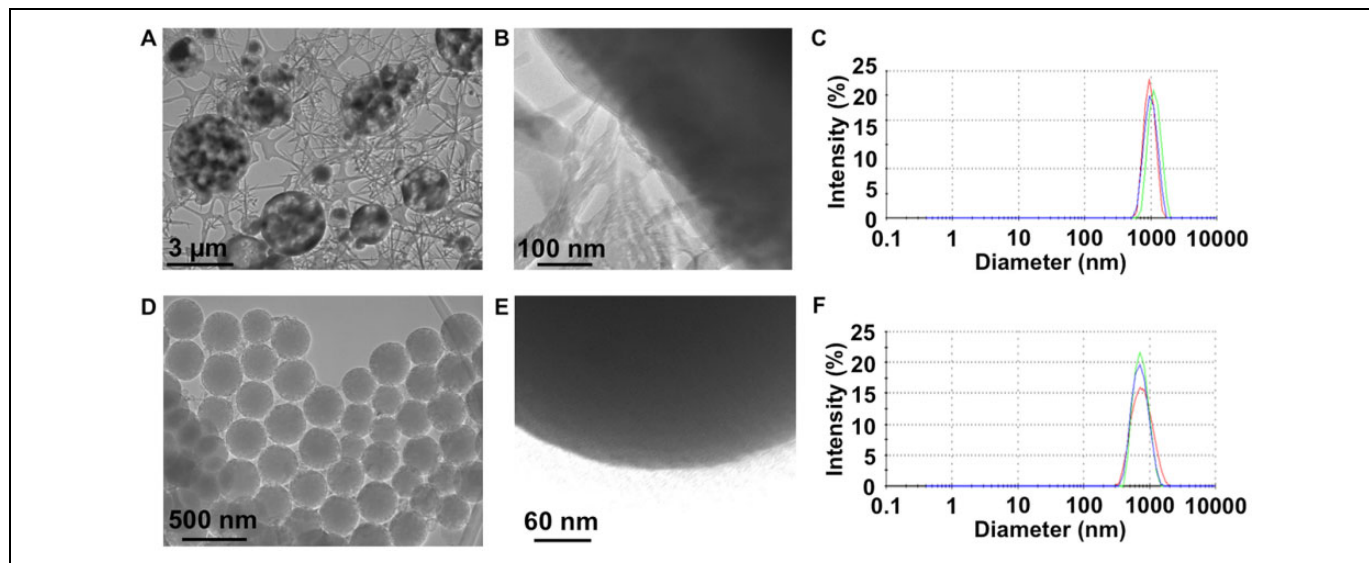


Figure 2. Particle characterizations. Iron oxide particles that were coated with polystyrene embedded with Dragon Green fluorophore were conjugated with protamine sulfate and glutamine. A, A TEM image showed that the particles were spherical. B, TEM images at higher resolution showed the coating. C, Dynamic light scattering measured an average diameter of 1840 ± 190 nm for these particles. Mesoporous silica particles were synthesized using the Stöber method, loaded with Alexa Fluor 647, and conjugated with protamine sulfate and glutamine. D, The TEM image showed that the particles were spherical. E, The TEM image showed a thin coating on these particles. F, Dynamic light scattering measured an average diameter of 760 ± 10 nm for these particles. TEM indicates transmission electron microscopy.

Transmission electron microscopy (TEM) was performed with a Phillips (FEI) CM12S microscope operating at 80 kV that provided 8-bit TIFF images collected with an AMT Optonics 4 Mpixel camera. Some TEM images were obtained with a 200-kV Hitachi H8100 microscope with a high brightness LaB6 electron source that captured images on film.

To perform SEM, tissue samples were placed in 4% paraformaldehyde at 4°C for at least 4 hours and then dehydrated with ethanol gradients from 70% to 100% in 5% increments.²⁶ Particles and reperfused liver tissue were coated with gold on a Hummer sputtering system (Anatech USA, Inc, Union City, California). Tissue samples were placed onto a glass slide, mounted on the SEM stub, and placed in a gold coat sputtering chamber. Reperfused liver tissue that was fixed for 24 hours was placed on the SEM stub for gold coating. A 4-nm layer of gold was laid onto the particle sample by coating at 15 milliamps for 60 seconds. Iron oxide and silica particles were imaged with an S-4800 field emission SEM (Hitachi Corporation, Japan). Imaging was performed in a conventional vacuum at 30 kV, 3.0 spot sizes, from $\times 200$ to $\times 27\,000$ magnification, with an Everhart-Thornley detector. Images were analyzed using Inspect S software version 3.1.4 (FEI Co, Hillsboro, Oregon).

Results

Characterizations of the Particles

The mesoporous silica particles were synthesized using the Stöber method, which can use different mixtures of ammonia, ethanol, and TEOS to produce particles with different average sizes and size distributions.²⁷ The mixture used in our formulation

produced aggregated particle sizes with a homogenous Gaussian distribution of 760 ± 10 nm as determined with DLS (Figure 2). The TEM performed at 200 kV showed pore sizes of 1 to 5 nm for the mesoporous particles. For comparison, the characterization of the iron oxide particles showed a larger particle size of 1840 ± 190 nm. Confocal microscopy confirmed that the fluorescence intensities of both types of particles were not significantly changed after surface modification.

The signal amplitude from ultrasound imaging was linearly correlated with silica particle concentration from 0.2 to 1.56 mg/mL (Figure 3). The standard deviation of the background signal without silica particles was measured to estimate the noise level. Based on signal-to-noise ratio of $2\sqrt{2}$ that represents a 95% probability that the signal arises from the addition of silica particles to the sample, the minimum concentration of the mesoporous silica particles that can be reliably detected with ultrasound imaging is 0.28 mg/mL.²⁸

The r_2 relaxivity of iron oxide particles was determined to be $131 \text{ (mg/mL)}^{-1} \cdot \text{s}^{-1}$ (Figure 4). A decellularized mouse liver was imaged with MRI to estimate the endogenous signal amplitude. Using the same 95% probability threshold listed above, we determined that a minimum concentration of 0.080 mg/mL of iron oxide particles was required for detection with MRI. Therefore, MRI was 3.5 times more sensitive than ultrasound imaging for detecting their respective particles with our tested protocols.

Ultrasound Imaging of Liver

Ultrasound images of the liver were obtained with and without silica particles (Figure 5A). Images before perfusion of the

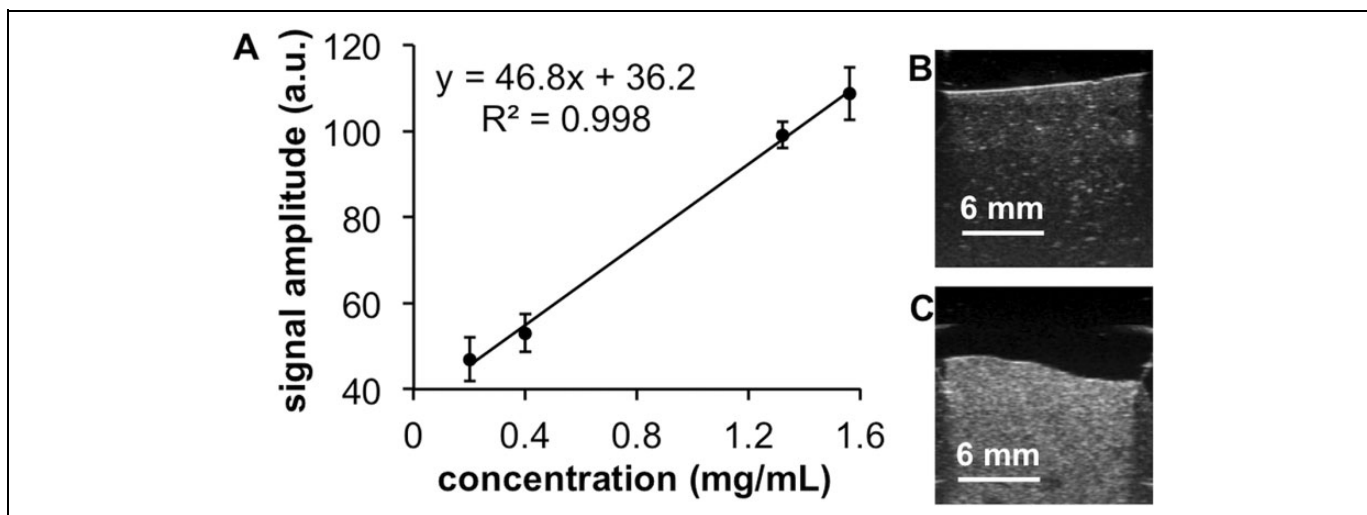


Figure 3. The relationship between ultrasound signal and silica particle concentration. A, The ultrasound signal amplitude was found to be linear with concentration. B, A sample of 0.2 mg/mL of the silica particle in 10% agar. C, A sample of 1.56 mg/mL of silica particle in 10% agar showed a difference in ultrasound signal amplitude.

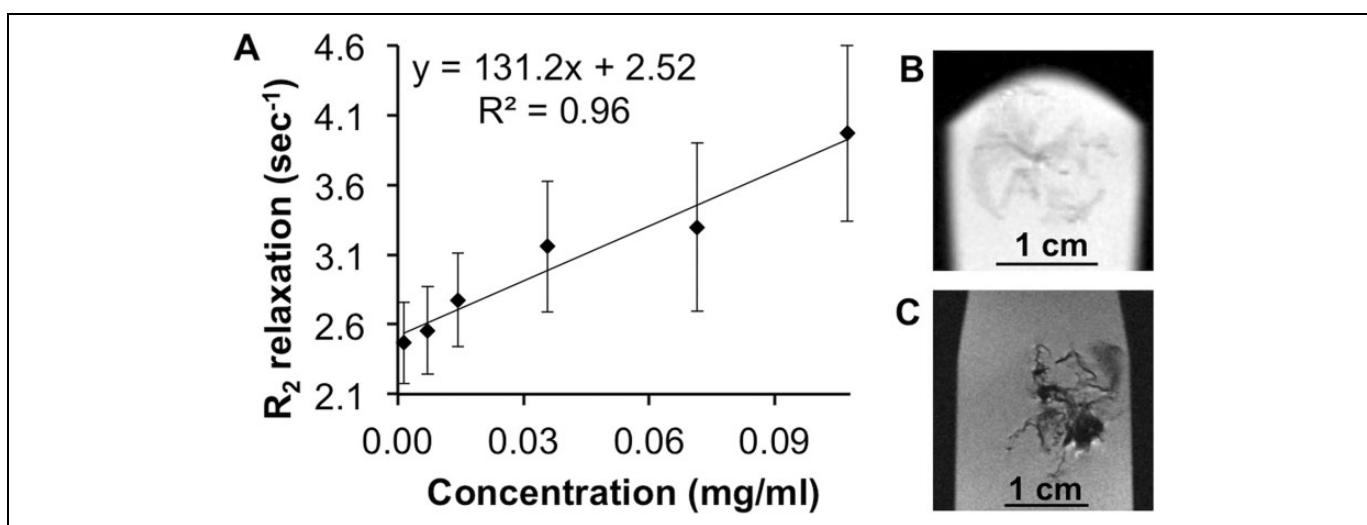


Figure 4. The relationship between iron oxide signal and iron oxide particle concentration. A, The R_2 relaxation rate was found to be linear with concentration. B, A decellularized liver without iron-labeled cells. C, A recellularized liver at day 31 with iron-labeled cells showed a difference in the T_2 -weighted MRI signal amplitude. MRI indicates magnetic resonance imaging.

silica-labeled cells showed some regions of higher signal amplitude that were indicative of vasculature. Most of these high-signal regions were near the center of the liver, where the inferior vena cava and portal veins enter the liver and spread through the lobes. After reseeding with approximately 1 million silica-labeled cells, the estimated density of cells or cell groups increased during the longitudinal study (Table 1), although a majority of cell growth occurred during the first 10 days (Figure 5B). The spatial resolution of the ultrasound images was 125 μm so that pixels with image signal indicative of mesoporous silica particles did not necessarily represent individual cells labeled with silica. Instead, these results suggested that ultrasound imaging underestimated the number of cells in the liver.

Magnetic Resonance Imaging of Liver

The MR images were taken of the liver with and without the iron oxide particles (Figure 6A). The image of the decellularized liver before the reperfusion of iron-loaded cells identified the protein scaffold but otherwise showed no evidence for iron oxide particles. The estimated density of cells or cell groups continuously increased during the longitudinal MRI study after reseeding with approximately 1 million cells, reaching the highest density at 31 days, at the end of the study (Figure 6B, Table 1). The MRI resolution was 54 μm so that pixels with image signal indicative of iron oxide did not necessarily represent individual cells labeled with iron oxide particles.

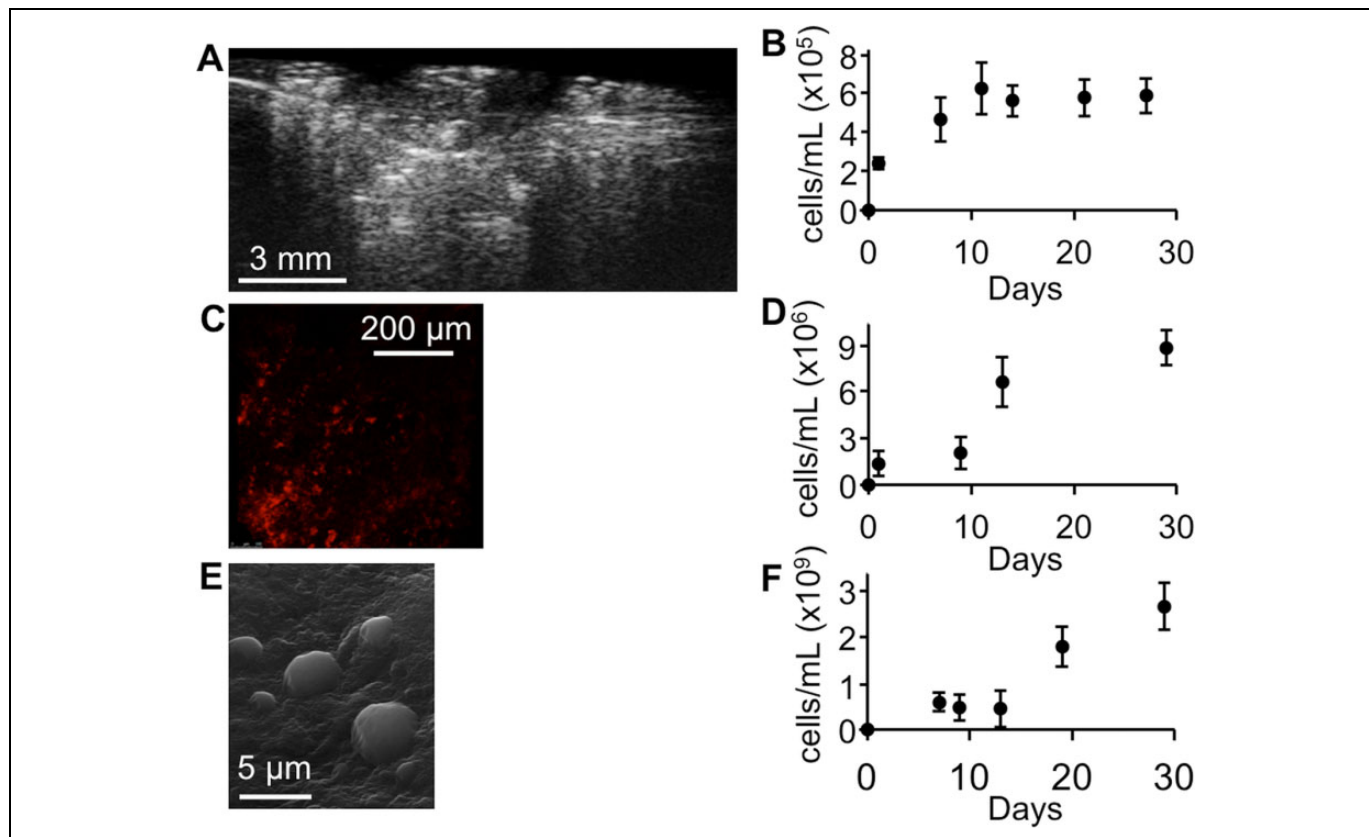


Figure 5. Liver recellularization with silica-labeled cells. A, An ultrasound image of the liver 27 days after reseeding shows signal from the silica particles. B, Ultrasound imaging tracked cell proliferation, which plateaued after 10 days. C, Confocal fluorescence microscopy of a liver biopsy sample detected the Alexa Fluor 647 fluorophore in the silica particles. D, Cell proliferation using fluorescence. E, SEM of a liver biopsy sample detected individual cells. F, SEM cell proliferation. SEM indicates scanning electron microscopy.

Table 1. Imaging-Based Detection of Labeled Cells.

Modality	Silica-Labeled Cells		Iron-Labeled Cells		Maximum Relative to SEM
	After 24 Hours	Maximum Number	After 24 Hours	Maximum Number	
Ultrasound	20 437	53 182	–	–	0.022%
MRI	–	–	275 512 ± 105 187	1 653 750 ± 329 700	1.22%
Confocal microscopy	117 900 ± 70 400	767 800 ± 99 600	1 231 000 ± 285 000	14 994 000 ± 1 570 000	0.32% (silica), 11.1% (iron)
SEM	–	237 500 000 ± 45 300 000	–	134 700 000 ± 1 600 000	–

Abbreviations: MRI, magnetic resonance imaging; SEM, scanning electron microscopy.

Confocal Microscopy of Liver

Liver biopsies were imaged by confocal fluorescence microscopy to estimate total cell counts (Figures 5C and D and 6C and D; Table 1). Similar to ultrasound imaging and MRI, confocal imaging showed a consistent increase in the number of cells or cell groups over time. Also, confocal microscopy detected more cells or cell groups in liver reseeded with iron-labeled cells than with silica-labeled cells. This result agreed with the detection of more cells or cell groups with MRI relative to ultrasound imaging. Furthermore, the number of cells or cell groups detected with confocal fluorescence microscopy

was greater than detection with ultrasound imaging and MRI, which may reflect the finer spatial resolution offered by confocal microscopy relative to the other imaging modalities.

Scanning Electron Microscopy of Liver

The SEM images were used to detect each cell in the field of view, which was then used to estimate total cell density throughout the liver (Figures 5E and F and 6E and F; Table 1). The SEM images were only acquired at the end point of each study. The SEM images were used to directly compare a reseeded liver with a control liver that was not decellularized

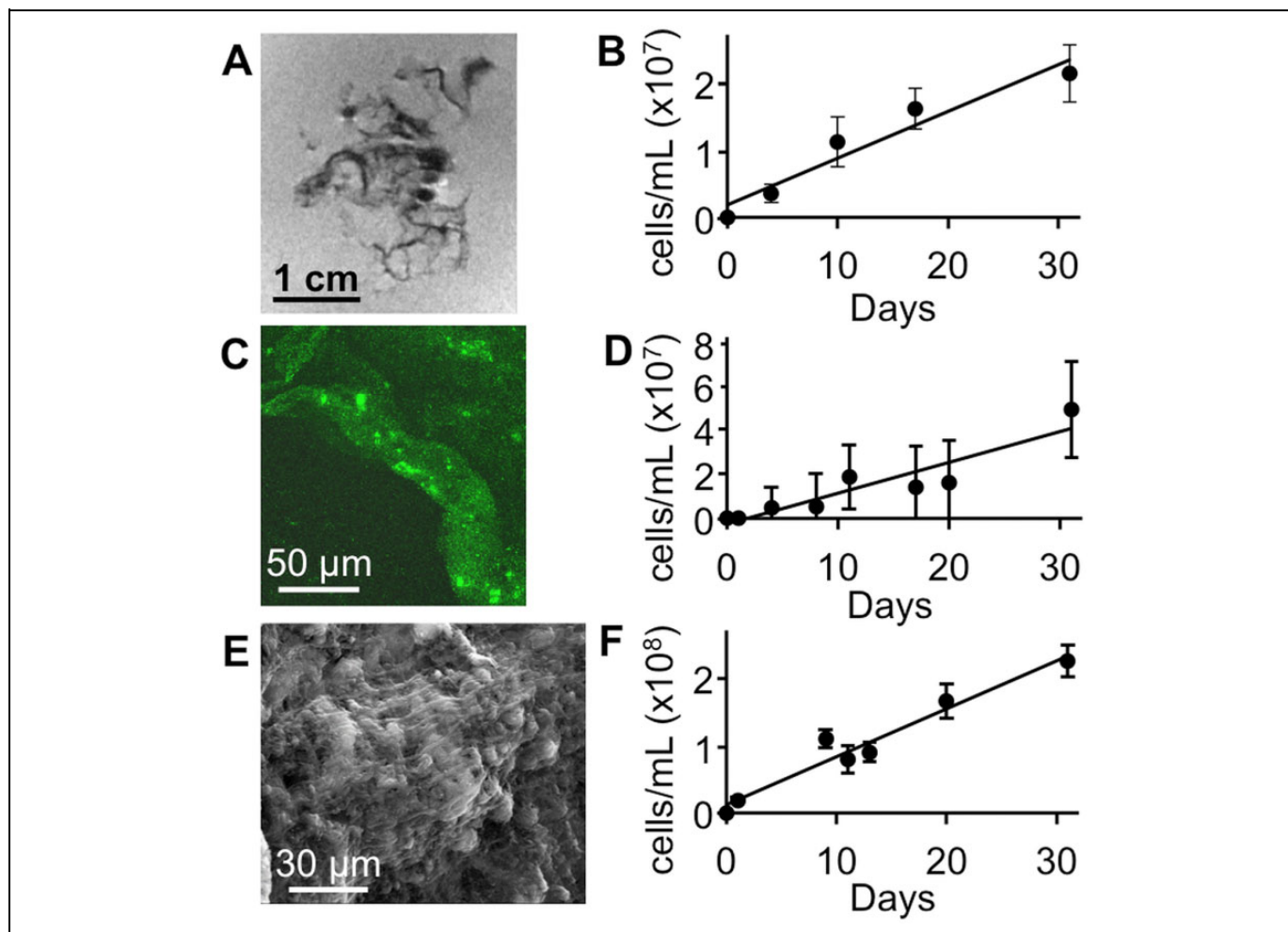


Figure 6. Liver recellularization with iron-labeled cells. A, An R_2 -weighted MRI image of the liver 31 days after reseeding showed signal from the iron oxide particles. B, MRI tracked cell proliferation, which was approximately linear during the time frame of the study. C, Confocal fluorescence microscopy of a liver biopsy sample detected the Green Dragon fluorophore. D, Confocal microscopy tracked cell proliferation. E, SEM of a liver biopsy sample detected individual cells 31 days after recellularization. F, SEM was also used to track cell proliferation. MRI indicates magnetic resonance imaging; SEM, scanning electron microscopy.

or reseeded. The cell density of the reseeded liver closely matched the density of the control liver. Assuming that SEM is the most accurate method for estimating cell count, ultrasound imaging estimated 0.022% of the total cell count, MRI estimated 1.22% of total cell count, and confocal microscopy estimated 0.32% to 11.1% of total cell count.

Final Status of the Particles

Particles were characterized after 31 days in cells (Figure 7). The silica particles decreased 90% in average diameter to 78 ± 7 nm, while the iron oxide particles decreased 84% in size to $290 \text{ nm} \pm 140$ nm. These results indicated that both types of particles had eroded.

Discussion

Ultrasound imaging, MRI, and confocal fluorescence microscopy underestimated the number of proliferating cells relative

to results from SEM. This underestimation likely resulted from the presence of multiple cells per imaging voxel for each of the imaging modalities. This underestimation was most severe for ultrasound imaging, which had the poorest spatial resolution of the imaging methods that were tested. For comparison, previous studies with very dilute concentrations of labeled cells could accurately detect each labeled cell.^{7,29,30} The reseeding process created a concentration of cells that did not allow for individual cell detection within the liver. Despite this underestimation, each of the imaging methods could successfully track the longitudinal progression of recellularization of the liver scaffold.

Cell proliferation within the reseeded liver scaffolds would be expected to increase the number of image voxels that are occupied by particle-labeled cells. Conversely, cell division would be expected to dilute the concentration per cell of the mesoporous silica particles or iron oxide particles. Our observed increase in the R_2 relaxation rate and the ultrasound

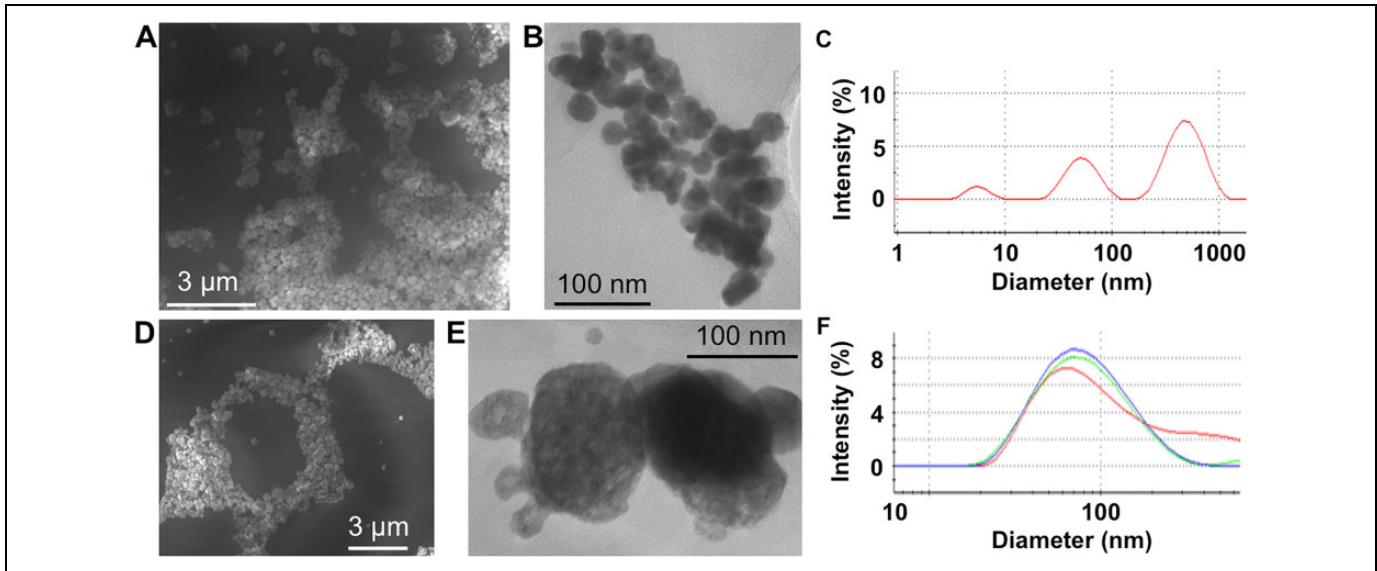


Figure 7. Particle degradation. A, SEM images showed a reduced size for the iron oxide particles. B, The TEM image showed reduced iron and polystyrene composition. C, Dynamic light scattering showed 3 distinct populations of materials, with an average diameter of 290 ± 139 nm, which was an 84.1% decrease in average diameter. D-F, A similar analysis of mesoporous silica particles showed an average diameter of $78 \text{ nm} \pm 7$ nm. SEM indicates scanning electron microscopy; TEM, transmission electron microscopy.

imaging signal throughout the reseeded liver scaffold suggested that the effect of cell proliferation was greater than the effect of dilution on imaging signals during the time course of our studies. A longer time course of a future study may show that continued cell division with a slowing of proliferation can dilute the concentration of particle per cell, eventually leading to a decrease in R_2 relaxation rate and ultrasound imaging signal.

Based on these results, future studies should consider using MRI for tracking the recellularization of decellularized organs. Magnetic resonance imaging was able to detect a 3.5-fold lower level of iron oxide labels in cells relative to intracellular silica labels. The MR images were obtained with better spatial resolution that generated higher counts of cells or cell groups relative to the more coarsely resolved ultrasound images. More generally, MRI has a greater depth of view for larger tissues than ultrasound imaging, even with a high frequency ultrasound imaging probe, which may be an advantage when scaling this method to larger liver samples. Although clinical ultrasound imaging is known to be faster than clinical MRI studies, the ultrasound imaging and MRI protocols and image processing for this study were comparable in time and effort.

The analysis of liver scaffolds reseeded with iron-labeled cells showed a higher number of cells than scaffolds reseeded with silica-labeled cells. Furthermore, the proliferation of iron-labeled cells was more sustained than with silica-labeled cells, which plateaued in proliferation 10 days after reseeded. The presence or degradation of the silica particles may have led to the lower proliferation of these cells, considering that the cell isolation and reseeded of liver scaffolds were identical for both types of labeled cells. The average diameters of the particles were also different, which may have also led to

differences in cell proliferation. More generally, the toxicity potentially caused by intracellular particles remains an active area of research.³¹⁻³³ The noninvasive imaging modalities investigated in this study may be useful tools for monitoring the longitudinal progression of cell proliferation in many organ scaffolds to evaluate potential toxicities of additional particle formulations.^{34,35}

Acknowledgments

The authors thank Dr Craig Aspinwall of the University of Arizona for helpful discussions.


Declaration of Conflicting Interests

The author(s) declared no potential conflicts of interest with respect to the research, authorship, and/or publication of this article.

Funding

The author(s) disclosed receipt of the following financial support for the research, authorship, and/or publication of this article: The authors acknowledge funding through NIH grants P30 CA023074 and P50 CA95060. J.E.K. was supported by the United States Army Advanced Civil Schooling Program and the West Point Faculty Development Research Fund. I.A.C. was supported by a TRIF imaging fellowship at the University of Arizona and NIH grant R21 EB019133.

ORCID iD

Douglas W. Cromeley  <http://orcid.org/0000-0003-2193-4139>

References

1. Ebrahimi A, Rahim F. Recent immunomodulatory strategies in transplantation. *Immun Invest*. 2014;43(8):829–837.

2. Weiss TS, Lichtenauer M, Kirchner S, et al. Hepatic progenitor cells from adult human livers for cell transplantation. *Gut*. 2008; 57(8):1129–1138.
3. Song GW, Lee SG. Living donor liver transplantation. *Curr Opin Organ Transplantation*. 2014;19(3):217–222.
4. Radwan MM, Radwan BM, Nandipati KC, Hunter WJ III, Agrawal DK. Immunological and molecular basis of nonalcoholic steatohepatitis and nonalcoholic fatty liver disease. *Expert Rev Clin Immunol*. 2013;9(8):727–738.
5. Akamatsy N, Sugawara Y, Kokudo N. Living donor liver transplantation for patients with hepatocellular carcinoma. *Liver Cancer*. 2014;3(2):108–118.
6. Rumack CM, Wilson SR, Charboneau JW. *Diagnostic Ultrasound*. New York, NY: Mosby; 1998.
7. Liu J, Levine AL, Mattoon JS, et al. Nanoparticles as image enhancing agents for ultrasonography. *Phys Med Biol*. 2006; 51(9):2179–2189.
8. Rosenholm JM, Zhang J, Linden M, Sahlgren C. Mesoporous silica nanoparticles in tissue engineering—a perspective. *Nanomedicine*. 2016;11(4):391–402.
9. Hakke EM, Brown RW, Thompson MR, et al. *Magnetic Resonance Imaging: Physical Principles and Sequence Design*. New York, NY: John Wiley & Sons; 1999.
10. Yoo B, Pagel MD. An overview of responsive MRI contrast agents for molecular imaging. *Front Biosci*. 2008;13:1733–1752.
11. Hingorani DV, Bernstein AS, Pagel MD. A review of responsive MRI contrast agents: 2005–2014. *Contrast Media Mol Imaging*. 2015;10(4):245–265.
12. Liu W, Frank JA. Detection and quantification of magnetically labeled cells by cellular MRI. *Eur J Radiol*. 2009;70(2):258–264.
13. Rossi LM, Shi L, Quina FH, Rosenzweig Z, Stöber synthesis of monodispersed luminescent silica nanoparticles for bioanalytical assays. *Langmuir*. 2005;21(10):4277–4280.
14. Patil US, Qu H, Caruntu D, et al. Labeling primary amine groups in peptides and proteins with N-hydroxysuccinimidyl ester modified Fe₃O₄@SiO₂ nanoparticles containing cleavable disulfide-bond linkers. *Bioconjug Chem*. 2013;24(9): 1562–1569.
15. Ebert SN, Taylor DG, Nguyen HL, et al. Noninvasive tracking of cardiac embryonic stem cells in vivo using magnetic resonance imaging techniques. *Stem Cells*. 2007;25(11):2936–2944.
16. Strom SC, KD, Thompson MT, Pizarov LA, Nussrov AK. Large Scale Isolation and Culture of Human Hepatocytes. In: Franco D, Doudjema K, Varet K (eds). *Ilots de Langerhans et hepatocytes: Vers Une Utilisation Therapeutique*. Paris, France: Les Editions Inserm; 1998:195–205.
17. Mitry RR, Hughes RD, Dhawan A. Progress in human hepatocytes: isolation, culture & cryopreservation. *Semin Cell Dev Biol*. 2002;13(6):463–467.
18. Liu W, Hou Y, Chen H, et al. Sample preparation method for isolation of single-cell types from mouse liver for proteomic studies. *Proteomics*. 2011;11(17):3556–3564.
19. Gridelli B, Vizzini G, Pietrosi G, et al. Efficient human fetal liver cell isolation protocol based on vascular perfusion for liver cell-based therapy and case report on cell transplantation. *Liver Transpl*. 2012;18(2):226–237.
20. Smedsrod B, Pertoft H. Preparation of pure hepatocytes and reticuloendothelial cells in high yield from a single rat liver by means of Percoll centrifugation and selective adherence. *J Leukoc Biol*. 1985;38(2):213–230.
21. Smedsrod B, Pertoft H, Eggertsen G, Sundström C. Functional and morphological characterization of cultures of Kupffer cells and liver endothelial cells prepared by means of density separation in Percoll, and selective substrate adherence. *Cell Tissue Res*. 1985;241(3):639–649.
22. Castaneda RT, Khurana A, Khan R, Daldrup-Link HE. Labeling stem cells with ferumoxytol, an FDA-approved iron oxide nanoparticle. *J Vis Exp*. 2011;57:e3482.
23. Crapo PM, Gilbert TW, Badylak SF. An overview of tissue and whole organ decellularization processes. *Biomaterials*. 2011; 5(12):3233–3243.
24. Schneider CA, Rasband WS, Eliceiri KW. NIH Image to ImageJ: 25 years of image analysis. *Nature Methods*. 2012;9(7):671–675.
25. Boretius S, Kasper L, Tammer R, Michaelis T, Frahm J. MRI of cellular layers in mouse brain in vivo. *Neuroimage*. 2009;47(4): 1252–1260.
26. Meuillet EJ, Mania-Farnell B, George D, Inokuchi JI, Bremer EG. Modulation of EGF receptor activity by changes in the GM3 content in a human epidermoid carcinoma cell line, A431. *Exp Cell Res*. 2000;256(1):74–82.
27. Papa AL, Basu S, Sengupta P, et al. Mechanistic studies of Gemcitabine-loaded nanoplateforms in resistant pancreatic cancer cells. *BMC Cancer*. 2012;12:419.
28. Liu G, Ali M, Yoo B, Griswold MA, Tkach JA, Pagel MD. Paracet MRI with improved temporal resolution. *Magn Reson Med*. 2009;61(2):399–408.
29. Shapiro EM, Skrtic S, Sharer K, Hill JM, Dunbar CE, Koretsky AP. MRI detection of single particles for cellular imaging. *Proc Natl Acad Sci U S A*. 2004;101(30):10901–10906.
30. Hinds KA, Hill JM, Shapiro EM, et al. Highly efficient endosomal labeling of progenitor and stem cells with large magnetic particles allows magnetic resonance imaging of single cells. *Blood*. 2003; 102(3):867–872.
31. Arbab AS, Yocum GT, Rad AM, et al. Labeling of cells with ferumoxides-protamine sulfate complexes does not inhibit function or differentiation capacity of hematopoietic or mesenchymal stem cells. *NMR Biomed*. 2005;18(8):553–559.
32. van Buul GM, Farrell E, Kops N, et al. Ferumoxides-protamine sulfate is more effective than ferucarbotran for cell labeling: implications for clinically applicable cell tracking using MRI. *Contrast Media Mol Imaging*. 2009;4(5):230–236.
33. Perkins TN. Differences in gene expression and cytokine production by crystalline vs. amorphous silica in human lung epithelial cells. *Part Fibre Toxicol*. 2012;9(1):6.
34. Bonandrini B, Figliuzzi M, Papadimou E, et al. Recellularization of well-preserved acellular kidney scaffold using embryonic stem cells. *Tissue Eng Part A*. 2014;20(9-10):1486–1498.
35. Oberwallner B, Brodarac A, Anic P, et al. Human cardiac extracellular matrix supports myocardial lineage commitment of pluripotent stem cells. *Eur J Cardiothorac Surg*. 2015; 47(3):416–425.